Structural Basis of p75 Transmembrane Domain Dimerization*

Kirill D. Nadezhdin[‡1], Irmina García-Carpio[§1,2], Sergey A. Goncharuk[‡], Konstantin S. Mineev[‡], Alexander S. Arseniev[‡3,4], and ⓘD Marçal Vilar[§3,5]

From the ‡Shemyakin-Ovchinnikov Institute of Bioorganic Chemistry of the Russian Academy of Sciences, Moscow 117997, Russian Federation and §Neurodegeneration Unit, Unidad Funcional de Investigación de Enfermedades Crónicas-Instituto de Salud Carlos III, Crta Majadahonda a Pozuelo km.2 Majadahonda, Madrid 28220, Spain

Dimerization of single span transmembrane receptors underlies their mechanism of activation. p75 neurotrophin receptor plays an important role in the nervous system, but the understanding of p75 activation mechanism is still incomplete. The transmembrane (TM) domain of p75 stabilizes the receptor dimers through a disulfide bond, essential for the NGF signaling. Here we solved by NMR the three-dimensional structure of the p75-TM-WT and the functionally inactive p75-TM-C257A dimers. Upon reconstitution in lipid micelles, p75-TM-WT forms the disulfide-linked dimers spontaneously. Under reducing conditions, p75-TM-WT is in a monomer-dimer equilibrium with the Cys[257] residue located on the dimer interface. In contrast, p75-TM-C257A forms dimers through the A*XXX*G motif on the opposite face of the α-helix. Biochemical and cross-linking experiments indicate that A*XXX*G motif is not on the dimer interface of p75-TM-WT, suggesting that the conformation of p75-TM-C257A may be not functionally relevant. However, rather than mediating p75 homodimerization, mutagenesis of the A*XXX*G motif reveals its functional role in the regulated intramembrane proteolysis of p75 catalyzed by the γ-secretase complex. Our structural data provide an insight into the key role of the Cys[257] in stabilization of the weak transmembrane dimer in a conformation required for the NGF signaling.

The neurotrophins (NTs)[6] are a family of neurotrophic factors that control multiple aspects of nervous system development and function. NTs interact with two distinct receptors, a cognate member of the Trk receptor tyrosine kinase family and the p75 neurotrophin receptor, a member of the tumor necrosis factor (TNF) receptor superfamily of death receptors (1). The most prominent biological function of p75 may be the induction of cell death, although it demonstrates several other activities, like survival, axonal growth, and cell migration (2–5).

The precise mechanism as to how p75 transmits diverse signals in the normal or diseased nervous system remains elusive (3). Signal transduction by p75 is thought to proceed via the ligand-dependent recruitment and release of protein interactors to and from the receptor (6). Although different oligomer species have been recently described as the active receptor (7–10), several lines of evidence support the dimeric nature of p75 in neurotrophin signaling. NTs are homodimers in solution (11) that dimerize the extracellular domain of p75 upon binding as seen by *in vivo* cross-linking (12), by x-ray crystallography (13, 14), and in solution (15). Engineered cysteine constructs activate p75 in the absence of NGF by inducing constitutive dimers (7), and the extracellular (16) and the intracellular domain (17, 18) form stable dimers in solution. In addition, the TM domain of p75 self-associates as measured by ToxCAT (8). All these data are supported by FRET (8, 9) and by β-galactosidase protein-protein interaction assays (19), indicating that in the absence of NTs a significant fraction of p75 exists as preformed dimers on the plasma membrane.

Like several single span transmembrane receptors (20) p75 dimerization is not enough for its activation, and only specific disulfide-linked dimers, mediated by Cys[257] in the TM domain, respond to NGF binding (8). Although the p75-C257A mutant is still capable to form dimers and bind to NGF (8), it is unable to transduce the signals triggered by NGF binding in some cell signaling paradigms (8). In addition, p75-C257A is less prone to γ-secretase processing (9) and has a reduced level of interaction with the Nogo receptor (17). To provide insight into the conformation of p75 TM domain active disulfide dimers *versus* p75-C257A inactive dimers, here we describe the high resolution NMR structure of the p75-WT and -C257A transmembrane domains.

Experimental Procedures

DNA Construct Design—p75 was expressed from the pcDNA3 vector backbone (Invitrogen) using a full-length coding sequence flanked by an N-terminal hemagglutinin (HA) epitope tag. Mutations were introduced by direct mutagenesis

The atomic coordinates and structure factors (codes 2mic and 2mjo) have been deposited in the Protein Data Bank (http://wwpdb.org/).

[6] The abbreviations used are: NT, neurotrophin; TM, transmembrane; DPC, dodecylphosphocholine; Tricine, *N*-[2-hydroxy-1,1-bis(hydroxymethyl)ethyl]glycine; LPR, lipid to protein ratio; HSQC, heteronuclear single quantum coherence; TROSY, transverse relaxation optimized spectroscopy; TOCSY, total correlation spectroscopy; MBP, maltose-binding protein; PMA, phorbol 12-myristate 13-acetate; CTF, C-terminal fragment; ICD, intracellular domain; GpA, glycophorin A.

using *Pfu* Turbo DNA polymerase (Agilent), and the oligonucleotide sequences are available upon request.

Constructs of p75 TM for Cell-free Expression—The gene encoding the transmembrane and juxtamembrane residues 245–284 (MT[245]RGTTDNLIPVYCSILAAVVVGLVAYIAFK-RWNSSKQNKQ[284]) of human p75 receptor (p75-TM-WT and the C257A point mutant form of p75 TM (p75-TM-C257A)) was amplified by PCR from six chemically synthesized oligonucleotides (Evrogen, Russia) partially overlapped along its sequence. p75-TM-C257A was obtained by site-directed mutagenesis by PCR. All constructs contained a mutation in the palmitoylation site C279A to avoid the undesirable intermolecular disulfide cross-linking. In our previously published work with a longer construct of p75NTR (21), both the wild-type and C279A variants were studied, and no difference in the NMR spectra of the TM region were observed in both dodecylphosphocholine (DPC) micelles and dimyristoylphosphatidylcholine/dihexanoylphosphatidylcholine bicelles.

Cell-free Gene Expression—Bacterial S30 cell-free extract was prepared from the *Escherichia coli* Rosetta (DE3) pLysS strain from 10 liters of cell culture according to the previously described protocol (22–24). The continuous exchange mode with 12.5-kDa membrane was used in this study (23). Preparative scale reactions (2–3 ml of reaction mixture) were carried out in 50-ml tubes. Optimal reaction conditions such as Mg^{2+} and K^+ concentrations, ratio of reaction mixture to feeding mixture, and DNA concentration were established using homemade reactors based on the mini-continuous exchange *E. coli* cell-free reactor previously described (22, 23). The final standard feeding mixture:reaction mixture ratio was 8:1, and the final cell-free reaction mixture contained 100 mM HEPES, 0.83 mM EDTA, KOH at pH 8.0, 0.1 mg/ml folinic acid, 20 mM acetylphosphate, 1.2 mM ATP, and 0.8 mM each of G/C/UTP, 2 mM 1,4-dithiothreitol, 0.05% sodium azide, 2% PEG 8000, 20 mM magnesium acetate, 270 mM potassium acetate, 60 mM creatine phosphate, 1 mM each of 20 amino acid or 0.25% of 20-amino acid mixture (Cambridge Isotope Laboratories), one tablet/50 ml Complete protease inhibitor (Roche Applied Science), 0.5 mg/ml *E. coli* tRNA (Roche Applied Science), 0.25 mg/ml creatine kinase from rabbit muscle (Roche Applied Science), 0.05 mg/ml T7 RNA polymerase prepared by a previously described protocol (24), 0.1 unit/μl Ribolock (Fermentas), 0.02 μg/μl plasmid DNA, and 30% S30 cell-free extract. All reagents were provided by Sigma unless otherwise specified. Plasmid DNA was purified using a Promega MaxiPrep kit. Reactions were conducted overnight at 34 °C and 150 rpm in an Innova 44R shaker (New Brunswick).

Protein Purification—Cell-free reaction mixture was diluted 3 times with buffer A (50 mM Tris, pH 8.0, and 200 mM NaCl). After 10 min of incubation, the mixture was centrifuged for 10 min at 18,000× g at room temperature. Precipitate was washed consecutively with buffer A containing 30 μg/ml RNase A (Fermentas) and buffer B (50 mM Tris, pH 8.0, and 100 mM NaCl). The target protein was solubilized with 200 μl of buffer B containing 1% lauryl sarcosine. After each step, the protein was centrifuged for 10 min at 18,000 × g at room temperature, and supernatant aliquots were analyzed by 12.5% Tricine SDS-PAGE (25).The clarified protein solution was applied onto a

10/300 Tricorn column prepacked with Superdex 200 (GE Healthcare) and pre-equilibrated with buffer B containing 0.2% lauryl sarcosine. Protein-containing fractions were combined and precipitated by a TCA/acetone procedure (26).

Preparation of NMR Samples in a Membrane-mimetic Medium—So-called "isotopic heterodimer" (1:1 mixture of unlabeled and ^{15}N/^{13}C-labeled peptides) samples were prepared for p75-TM-WT and p75-TM-C257A mutant to solve the structure. The peptide powders of both samples were first dissolved in 1:1 trifluoroethanol:H_2O mixture with addition of deuterated DPC (d_{38}, 98%; Cambridge Isotope Laboratories) and phosphate buffer, then kept for several minutes in an ultrasound bath, and lyophilized. After that dried samples were dissolved in 350 μl of 9:1 H_2O:D_2O mixture. To attain uniformity of the micelle size and distribution of the peptide throughout micelles, samples were stored in an ultrasound bath for several minutes until the solution was completely transparent. The p75-TM-WT concentration of the isotopic heterodimer sample was 1.9 mM, lipid to protein ratio (LPR) 50:1, pH 5.9, 20 mM phosphate buffer. The concentration of the mutant form p75-TM-C257A was 1.5 mM, LPR 50:1, pH 5.9, 20 mM phosphate buffer. Both samples were placed in Shigemi NMR tubes with glass plunger. To elucidate an LPR ratio for p75-TM-WT-C257A, an additional sample was prepared where only Gly, Phe, Leu, Ala, and Tyr residues were ^{15}N-labeled. These residues were observed to be the most sensitive to oligomerization. Selective residue labeling was implemented to avoid peak overlapping while processing the NMR spectra.

NMR Spectroscopy and Spatial Structure Calculation—NMR spectra were acquired at 45 °C on 600- and 800-MHz AVANCE III spectrometers (Bruker BioSpin, Germany) equipped with the pulsed field gradient triple-resonance cryoprobes. ^{1}H, ^{13}C, and ^{15}N resonances of p75-TM-WT and p75-TM-C257A were assigned with CARA software (27) using two- and three-dimensional heteronuclear experiments (28): ^{1}H/^{15}N HSQC, ^{1}H/^{15}N TROSY, ^{1}H/^{13}C HSQC, ^{1}H/^{15}N HNHA, ^{1}H/^{13}C/^{15}N HNCA, ^{1}H/^{13}C/^{15}N HN(CO)CA, ^{1}H/^{13}C/^{15}N HNCO, three-dimensional HCCH-TOCSY, and ^{13}C- and ^{15}N-edited NOESY-HSQC (recorded on 600- and 800-MHz spectrometers, respectively). Dimeric spatial structures were calculated with the CYANA 3.0 program (29) based on torsion angle restraints estimated from the chemical shift values with the standard protocol of the TALOS-N program (30) and intra- and intermonomeric NOE distance restraints derived through the analysis of three-dimensional ^{15}N- and ^{13}C-edited NOESY and ^{15}N/^{13}C-F1-filtered/F3-edited NOESY spectra (28) acquired for isotopic heterodimer samples. MOLMOL software was used to calculate the contact areas between the dimer subunits and to visualize the structures (31). Hydrophobic properties of the α-helices in the p75-TM-WT and p75-TM-C257A dimers were calculated using the molecular hydrophobicity potential approach implemented in the program PREDDIMER (32).

ToxRED Assays—Original plasmids for ToxRED experiments were kindly provided by Dr. W. Degrado (University of California, San Francisco) and used as described (33). The region encompassing p75 TM domain was cloned using PCR with oligonucleotides with HindIII and XhoI to amplify the region between Asp[250] and Trp[276] of p75. Plasmids encoding

ToxR(GpA)MBP, ToxR(p75TM)MBP, and different p75 mutants were transformed into *E. coli* MM39 cells and plated onto Luria-Bertani (LB) plates (with 50 μg/ml ampicillin). Colonies were inoculated into LB medium (with 50 μg/ml ampicillin). Fresh LB cultures (with 50 μg/ml ampicillin) were inoculated from fresh plates, grown at 37 °C until approximately an A_{600} of $\approx$0.6 was reached, and harvested by centrifugation. Cells were then lysed in lysis buffer (TNE, 50 mM Tris, pH 7.5, 150 mM NaCl, 1 mM EDTA) in gentle conditions to avoid mCherry denaturation. After transfer to 1.5-ml Eppendorf tubes, the mixture was incubated at room temperature with gentle agitation for 30 min. Samples were centrifuged for 10 min at 12,000 × *g* to remove cell debris and clarify supernatants for analysis. 150 μl of clarified supernatant were transferred to black optically clear 96-well plates. mCherry emission spectra were collected using a plate reader (Tecan, Maennedorf, Switzerland) with an excitation wavelength of 587 nm and emission wavelengths of 610–650 nm. Afterward, aliquots were transferred from black to clear 96-well plates, and the absorbance was measured from 450 to 750 nm. mCherry measurements and construct expression measurements were performed in at least 10 different colonies and were normalized for the relative expression level of each construct using Western blotting with MBP antibody. For Western blotting, samples were mixed with equal volumes of 2× SDS-PAGE sample buffer, heated to 95 °C for 10 min, separated on 10% (w/v) polyacrylamide minigels, blotted onto nitrocellulose membranes, and probed with MBP antibody. To analyze disulfide bond formation, bacteria colonies were lysed using TNE plus 10 mM iodoacetamide and run on non-reducing SDS-polyacrylamide gels.

In Vivo Cross-linking and Western Blotting Analysis—HeLa cells were transfected with the indicated p75 constructs. 48 h after transfection, cells were washed three time with cold PBS and then cross-linked with bis(sulfosuccinimidyl)suberate (Pierce) at 4 °C for 15 min. Afterward, cells were washed again three times with PBS and incubated for 30 min with 0.15 M glycine in 100 mM Tris-HCl, pH 7.5, to quench the cross-linker. Cells were washed in PBS and lysed in cold lysis buffer (50 mM Tris-HCl, pH 7.5, 150 mM NaCl, 1 mM EDTA, 0.1% SDS, 0.1% Triton X-100, 1 mM PMSF, 10 mM NaF, 1 mM Na$_2$VO$_3$, 10 mM iodoacetamide, and protease inhibitor mixture) at 4 °C. Cellular debris was removed by centrifugation at 13,000 × *g* for 15 min, and protein quantification was performed by Bradford assay. Proteins were resolved by SDS-PAGE, and membranes were incubated overnight at 4 °C with the following antibodies: rabbit polyclonal anti-human p75 (1:1000; reference number G3231, Promega). Following incubation with the appropriate secondary antibody, membranes were imaged using enhanced chemiluminescence and autoradiography.

p75 Cleavage Experiments—p75 cleavage experiments were carried out according to the protocol described previously by Kanning *et al.* (34). Briefly, 48 h after transient transfection, HeLa cells were incubated for 90 min with either 1 μM proteasome inhibitor epoxomicin (Sigma), 10 μM Compound E (Millipore), or PBS buffer. Next, 200 nM phorbol 12-myristate 13-acetate (PMA; Sigma) was added for 40 min. The cells were lysed and analyzed by SDS-PAGE and Western blotting using p75 antibody as before.

Results

NMR Structure of p75 Transmembrane Domain Dimers—p75-TM-WT, the 245–284 fragment of rat p75 (Fig. 1A, *underlined*), was produced in a cell-free system (23). We solubilized the peptide in DPC micelles. Upon reconstitution, p75-TM-WT monomers spontaneously and completely adopt a dimeric conformation through a Cys^{257}-Cys^{257} disulfide bond, which cannot be easily disrupted by addition of β-mercaptoethanol or other reducing agents (Fig. 1B). The ^{15}N HSQC spectrum of p75-TM-WT contains the expected number of crosspeaks, and there are no significant minor forms observed, indicating that approximately 100% of the peptide is in the dimeric state (Fig. 1C). The use of ^{13}C/^{15}N-filtered NOESY experiments allowed the direct detection of interhelical contacts, which were used to calculate the spatial structure of the dimer (Fig. 1D and Table 1). Secondary ^{13}Cα chemical shifts for Leu^{252} and Ile^{253} are about 0 ppm, suggesting a random coil conformation. Thus, Pro^{254} is the first residue of the TM helix, and Cys^{257} is located in the first turn of TM α-helix close to the water-lipid interface, which makes it accessible to the solvent. The α-helical region extends for ~36 Å (residues 254–276) and consists of an uncharged region, Pro^{254}–Phe^{273}, and includes positively charged Lys^{274} and Arg^{275} at the C terminus. According to the obtained structure, the dimerization of p75-TM-WT is driven by the Cys^{257}-Cys^{257} disulfide bond and is additionally stabilized by intermolecular van der Waals interactions between branched side chains of Leu^{260}, Val^{264}, Val^{265}, and Val^{268} and stacking interaction of Phe^{273} and Trp^{276} aromatic rings (Fig. 1D).

p75-TM-WT Is a Weak Dimer under Reducing Conditions—The formation of disulfide dimers is spontaneous and quantitative. To study the conformation of p75-TM-WT in the absence of a disulfide bond, we prepared different peptide samples. We were able to find more than 80% of the p75-TM-WT free of disulfide bonds with solubilization of the peptide in the presence of a nitrogen atmosphere and 20 mM DTT. Under these conditions, p75-TM-WT is in a monomer-dimer equilibrium that depends on the LPR (Fig. 2A). To assess the propensity of the protein for a non-covalent dimerization and to study the conformation of such a dimer, a set of titration experiments was performed (Fig. 2B) (35). This titration allowed us to measure a ΔG^0 (standard free energy of dimerization) equal to −0.9 kcal/mol (Fig. 2C). This suggests that p75-TM-WT dimer under reducing conditions is rather weak if we compare with other TM domain dimers like glycophorin A ($\Delta G^0 = -5 \div -3$ kcal/mol depending on membrane mimetic) (36–38), VEGFR2 ($\Delta G^0 = -5$ kcal/mol in DPC) (35), and ErbB4 ($\Delta G^0 = -1.4$ kcal/mol in 1:4 dimyristoylphosphatidylcholine/dihexanoylphosphatidylcholine bicelles) (35, 39), but it is in the order of FGFR3 TM dimerization ($\Delta G^0 = -1$ kcal/mol in 9:1 DPC:SDS mixture) (40). We determined which residues in p75-TM-WT experience chemical shift changes upon dimer formation. As we observed in Fig. 2D, several residues throughout the whole p75-TM-WT showed chemical shift changes, including Cys^{257}, suggesting that Cys^{257} may be a part of the non-covalent dimer interface.
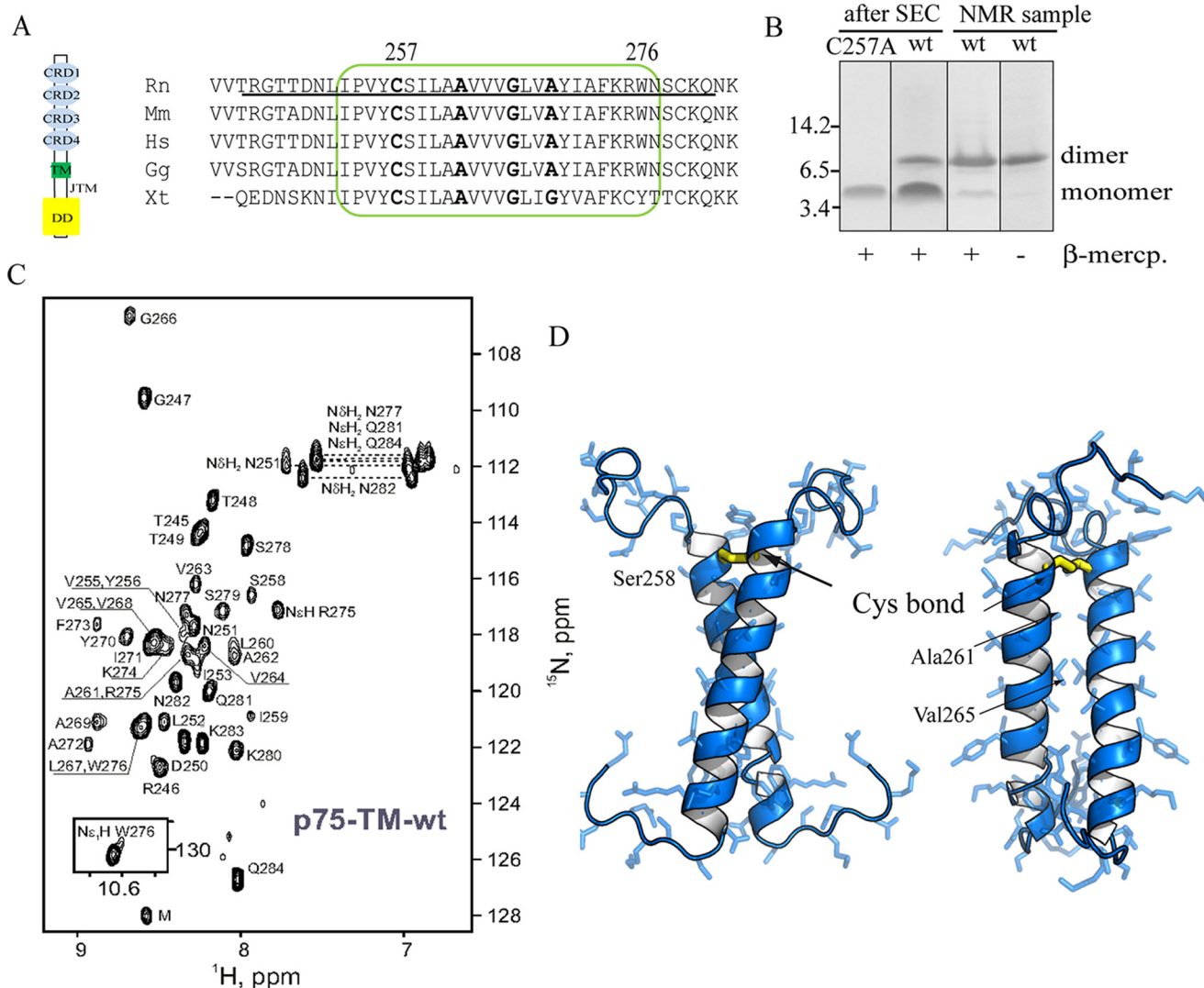
FIGURE 1. **Solution structure of the p75-TM-WT disulfide-linked dimer in DPC micelles.** *A*, schematic showing different p75 domains (*CRD*, cysteine-rich domains; *JTM*, juxtamembrane domain; *DD*, death domain) and the protein sequence alignment of the TM domain (*green box*). The protein sequence used for structural studies is *underlined*. *Rn*, *Rattus norvegicus*; *Mm*, *Mus musculus*; *Hs*, *Homo sapiens*; *Gg*, *Gallus gallus*; *Xt*, *Xenopus tropicalis*. *B*, SDS-PAGE analysis of p75 TM domain dimerization in 12% Tris-Tricine gel. *SEC*, size exclusion chromatography; *β-mercp*, *β*-mercaptoethanol. Bands are labeled as dimers or monomers on the *right*. Molecular weights are indicated on the *left*. *C*, ^{1}H/^{15}N HSQC spectrum of p75-TM-WT solubilized in an aqueous suspension of DPC micelles at an LPR of 50:1, 45 °C, and pH 5.9. ^{1}H-^{15}N backbone and side-chain resonance assignments are shown. *D*, schematic representation of the spatial structure of the p75-TM-WT dimer from three different angles: front, 90° rotation. The Cys^{257}-Cys^{257} disulfide bond is shown in *yellow*. The Protein Data Bank accession code for p75-TM-WT is 2mic.

Our data indicate that, when a free Cys^{257} is present, the disulfide bond is spontaneously formed, indicating that the Cys-Cys interface is conformationally explored very quickly. This suggests that Cys^{257} plays an important role in stabilizing weak p75 transmembrane dimers by the formation of a disulfide bond.

NMR Structure of the p75-TM-C257A Dimer—p75-C257A is inactive upon NGF binding, although it may form dimers as cross-linking studies suggested (8). We characterized the structure of the p75-TM-C257A by NMR in DPC micelles. We found that p75-C257A is in a monomer-dimer equilibrium (Fig. 3*A*) with a ΔG^0 equal to −1.8 kcal/mol (Fig. 3*B*), suggesting a stronger dimerization than p75-TM-WT. To have a deeper understanding of the structural basis of p75-C257A dimerization, we carried out chemical shift assignment in NMR spectra and structure calculation of p75-TM-C257A dimer. ^{15}N HSQC

spectra of p75-TM-WT and p75-TM-C257A mutant are similar and well dispersed (Fig. 3*C*). The three-dimensional structure showed that the p75-TM-C257A TM helical regions (Leu^{252}–Trp^{276}) associate in a left-handed parallel dimer via the A^{262}V*XX*G^{266}*XX*A^{269} motif (Fig. 3*D* and Table 1) in contrast to the p75-TM-WT dimerization that is right-handed. The motif A*XXX*G is conserved in all p75 sequences (Fig. 1*A*) and was previously suggested as a putative dimerization motif (7–9) due to the similarity to G*XXX*G motifs described in TM domain dimerization in several membrane proteins (41, 42). In addition dimerization of p75-TM-C257A occurs via the relatively polar part of the helical surface, and the C-terminal flank of the dimer is stabilized by intermolecular stacking interactions between aromatic rings of Phe^{273} residues. However, the observed mode of p75-TM-C257A dimerization does not correspond to the classical interaction via the G*XXX*G-like motifs. G*XXX*G-like

TABLE 1

Structural statistics for the 10 lowest target function NMR structures of the p75-TM dimer in the DPC micelles

	p75-TM-WT	p75-TM-C257A
NMR distance and dihedral restraints		
Total unambiguous NOE restraints	440	382
Intraresidue	78	128
Inter-residue	366	242
Sequential ($|i - j| = 1$)	174	134
Medium range ($1 < |i - j| < 4$)	178	96
Long range ($|i - j| > 4$)	14	12
Intermonomeric NOE	12	12
Hydrogen bond restraints (upper/lower)	84/84	102/102
Total torsion angle restraints	94	128
Backbone φ	42	52
Backbone ψ	42	52
Side chain χ^1	10	14
Structure calculation statistics		
CYANA target function (Å^2)	1.80 ± 0.35	2.40 ± 0.19
Average pairwise r.m.s.d., α-helical region 251–275 (Å)		
Backbone atoms	0.37 ± 0.09	0.38 ± 0.1
All heavy atoms	0.92 ± 0.17	0.92 ± 0.21
Ramachandran analysis[a]		
Residues in most favored regions (%)	75.0	88.9
Residues in additional allowed regions (%)	20.3	10.6
Residues in generously allowed regions (%)	4.4[b]	0.6
Residues in disallowed regions (%)	0.3[b]	0.0
Helix-helix packing		
Contact surface area per dimer subunit (Å^2)	400 ± 50	320 ± 40
Angle θ between the helix axes (°)	36 ± 5	66 ± 5
Distance d between the helix axes, region 251–275 (Å)	8.8 ± 0.5	7.2 ± 0.5

[a] Ramachandran statistics were determined using CYANA (29).
[b] Residues from unfolded and flexible regions.

motifs usually yield right-handed structures with the helix-crossing angles in the range of 30–50° in multihelical proteins (43). The left-handed arrangement with the helix-crossing angle equal to 66° found here may be a consequence of DPC micelles used as a membrane-mimetic. The lateral pressure of lipids in a bilayer and presence of the other TM helices would affect the dimerization and tend to decrease the crossing angle. Conversely, the GXXXG motif is not the paradigm for the helix-helix interactions. The mode of the interaction is determined by the properties of the surface of interacting helices. In our case, one can clearly observe that C257A helices interact via a relatively polar surface formed by the small-chain amino acids. In fact, Ala[262] is on the edge of the interface, and the real motif would look like AVXXGXXAYXXF, and the key feature of the interface is not only the polar interactions between Ala and Gly residues but also the stacking of aromatic rings. −40° would be obtained if the other surface, involving Ser[258], Ala[262], and Gly[266], is used.

The two obtained p75 TM dimer structures demonstrate striking differences (summarized in Table 1 and Fig. 4). Both structures have the same length of the TM helical region, ~36 Å (24 residues), but a significantly smaller crossing angle in p75-TM-WT compared with p75-TM-C257A (36° *versus* 66°, respectively) (Fig. 4*A*). The spatial distribution of the hydrophobic/hydrophilic properties of the p75-TM-WT dimer subunits, visualized by molecular hydrophobicity potential (44), reveals that the packing interface extends by around 400 Å^2 (per subunit) and is located alongside the polar regions of the TM helices (Table 1). Hydrophobicity plots in Fig. 4*B* show that the two TM dimers use different contact residues that are located on the opposing sides of the TM α-helix to dimerize: the p75-TM-WT dimer interface is C[257]XXXA[261]XXXV[265], and the

p75-TM-C257A dimer interface is A[262]V[263]XXG[266]XXA[269]. Some residues participate in both dimer interfaces, suggesting that the two dimer interfaces are mutually exclusive.

The AXXXG Motif Is Not Mediating p75-TM-WT Dimerization—We used ToxRED, a variation of the ToxCAT system (33, 45), to monitor p75 TM domain dimerization in bacterial membranes (Fig. 5). In ToxRED, dimerization of the TM regions can be monitored by the activation of the reporter gene mCherryFP (33). For that purpose, we introduced different mutations to the TM domain of p75, substituting the residues to isoleucine, a more bulky residue (Fig. 5*A*). p75-TM-A262I and p75-TM-G266I dimerize to a similar extent as p75-TM-WT, suggesting that the contribution of the motif AXXXG to p75 dimerization in this system is small (Fig. 5*B*). In contrast, p75-C257I mutant forms dimers that are completely disrupted by the double mutation p75-TM-C257I/G266I (Fig. 5*B*). This confirms the NMR data, indicating that dimerization of p75-TM-C257A is mediated by the AXXXG motif.

We then studied the dimerization of the full-length p75 in the plasma membrane of transfected mammalian HeLa cells by *in vivo* cross-linking using bis(sulfosuccinimidyl) suberate, which does not cross the plasma membrane (Fig. 5*C*). Upon transfection of the HeLa cells with the full-length p75, we observed the presence of cross-linked dimers (Fig. 5*C*). The amount of cross-linked dimers does not increase upon stimulation with NGF (100 ng/ml), suggesting that p75 forms preformed constitutive dimers in line with previous reports (8, 9, 19). Mutation of the Cys[257] does not disrupt p75 full length dimerization. Similarly, mutation of the AXXXGXXA motif residues to isoleucines, mutant p75-AGA, has no effect on the p75-WT dimerization (Fig. 5*C*), indicating that this motif does not play an important role in p75 full length dimerization in cells. However, when we mutated both Cys[257] and the AGA motif (mutant p75-C/AGA), we found a significantly smaller amount of the bis(sulfosuccinimidyl) suberate-cross-linked dimers (Fig. 5*C*), which is in line with the ToxRED and NMR data.

These results support that the dimerization of p75-C257A is mediated by the AXXXG motif in bacterial and mammalian membranes. p75-WT dimerization, by contrast, is independent of the AXXXG motif as we observed by NMR, ToxRED, and cross-linking. Based on this, we suggest that the conformation adopted by the C257A mutant may not reflect a native structure of p75.

Role of AXXXG Motif in p75-regulated Intramembrane Proteolysis—Although the GXXXG motifs are known to promote the homo- and heterodimerization of transmembrane domains (41), recent evidence suggests that several GXXXG-containing TM domains interact via alternative interfaces involving hydrophobic, polar, or aromatic residues (46). This is the case for p75-WT as the AXXXG motif does not mediate the p75 homodimerization. However, because the AXXXG motif is conserved in p75 sequences of different species, it is still possible that the motif is relevant in other functions of p75. p75 undergoes receptor intramembrane proteolysis (Fig. 6*A*), and although the role of receptor intramembrane proteolysis in p75 signaling is still debated, it has been proposed that cleavage is important for the biological functions of p75 (47–50). Recently
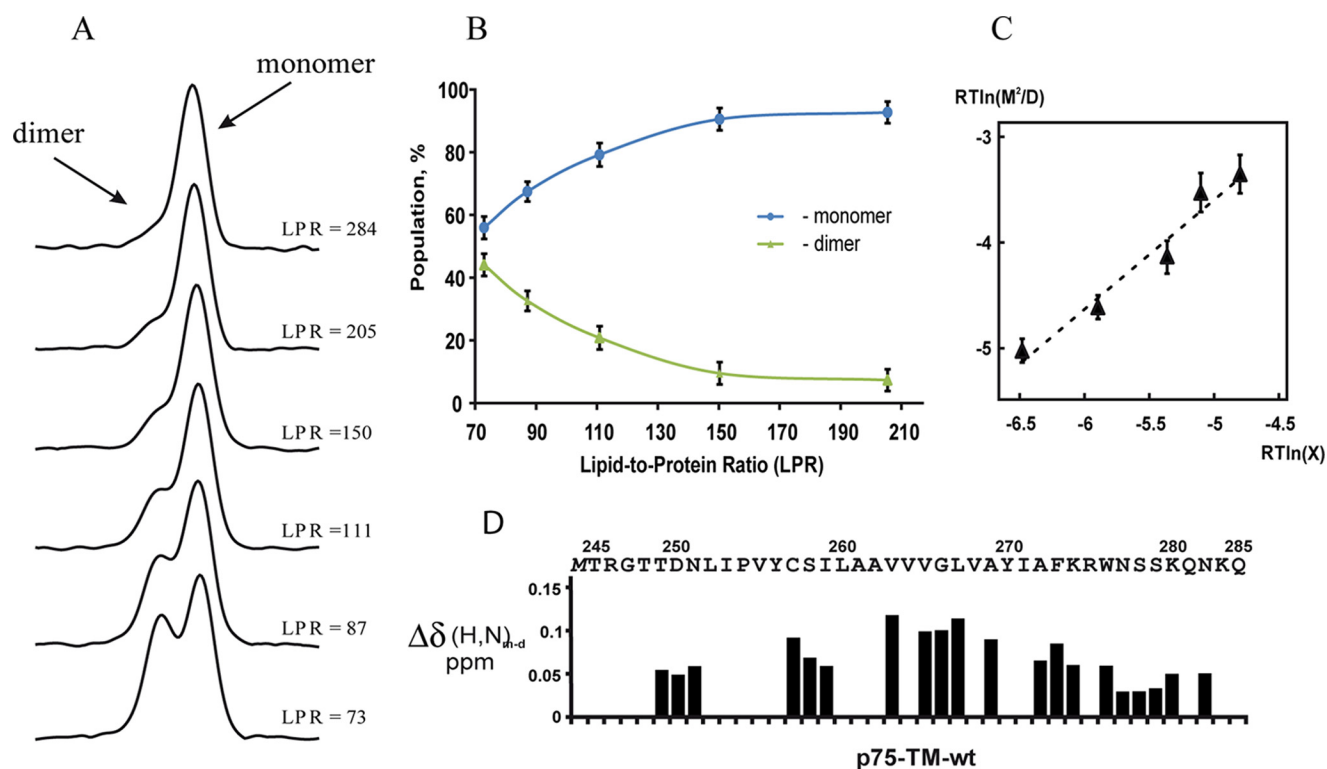
FIGURE 2. **Dimerization of p75-TM-WT in reducing conditions.** *A*, dimer-monomer population values were calculated from the integrals of cross-peak projections in the $^1H/^{15}N$ TROSY spectra. *B*, percentage of the monomeric (*blue*) and dimeric (*green*) p75-TM-WT forms at different LPRs. *C*, calculation of the apparent free energy of dimerization of p75-TM-WT. $\Delta G_{app} = RT\ln([M]2/[D])$ as a function $RT\ln(X)$ where $X = ([Det] - Nm[M] - Nd[D])/Ne$. $[M]$, $[D]$, and $[Det]$ represent monomer, dimer, and DPC concentration, respectively; Ne represents the number of DPC molecules per empty micelle; and Nm and Nd represent the number of DPC molecules per micelle containing monomer and dimer, respectively. *D*, chemical shift changes observed in p75-TM-WT dimerization in 20 mM DTT after titration at different LPRs. *Error bars* represent S.E.

Sykes *et al.* (9) found that mutation of the A*XXX*G motif to L*XXX*L reduces p75 intramembrane proteolysis in HEK293 and PC12 cells. This suggests that the A*XXX*G motif may play a role in the recognition or the cleavage of the p75 by the γ-secretase complex. Here, based on our structural studies, we investigated whether the cleavage process differs for various p75 mutations in the TM domain.

Shedding of the extracellular domain of p75 is a pre-requisite for γ-secretase cleavage (60). Treatment with the phorbol ester PMA, a metalloprotease activator that induces p75 shedding, resulted in the generation of a p75 C-terminal fragment (p75-CTF), which is the proper substrate for the γ-secretase complex. p75 intracellular domain (p75-ICD) is generated by the cleavage of p75-CTF, a process that is inhibited by the γ-secretase inhibitor Compound E (Fig. 6*B*). Treatment with epoxomicin, a proteasome inhibitor, helps to stabilize the p75-ICD, which is otherwise rapidly degraded, and permits quantification of γ-secretase activity via the p75-ICD to p75-CTF ratio, a direct measure of the γ-secretase processing (Fig. 6, *C* and *D*). HeLa cells were transfected with p75-WT and mutant constructs and treated with PMA for 40 min as described previously (34). The [p75-ICD]:[p75-CTF] ratio of p75-C257A was significantly lower than that of p75-WT, suggesting attenuated γ-secretase activity (Fig. 6*D*). A stronger effect is observed in the p75-AGA mutant (Fig. 6*D*), which is almost resistant to the action of the γ-secretase. The mutant p75-C/AGA with mutations in the Cys[257] and the AGA motif, also is less processed by the γ-secretase complex. These results suggest that the small

residues that comprise the A*XXX*G*XX*A motif are important for recognition and/or cleavage by γ-secretase rather than p75 homodimerization as we and others suggested previously (7, 9).

Discussion

We carried out our studies using solution NMR in detergent micelles that do not always properly simulate the properties of a real bilayer. Nanodiscs or bicelles are believed to better reflect the lipid bilayer characteristics (47, 48). However, micelles provide the smallest particles, which is of great importance for solution NMR spectroscopy. Therefore spatial structures obtained in micelles are of the best quality but may be non-physiological. Conversely, alternative membrane mimetics are also models of the lipid bilayer; lipid properties in nanodiscs and bicelles do not correspond to those in liposomes (51), and nanodiscs still cannot be used to solve the structures of transmembrane dimers due to their extremely large size. The bilayer thickness and state of the lipids are almost never known for a certain protein, so there always exists the possibility that incorrect choice of lipids in bicelles, nanodiscs, or liposomes can affect the state of the transmembrane protein, whereas micelles are much more flexible and can adopt their shape to the hydrophobic length of a transmembrane α-helix. Recent studies that were carried out for the same proteins (Bnip3 and glycophorin A) in micelles, bicelles, and sometimes lipid bilayers did not reveal any significant differences in the interfaces of helix-helix interactions in transmembrane dimers (52–55). However, pronounced differences were observed when the membrane-active
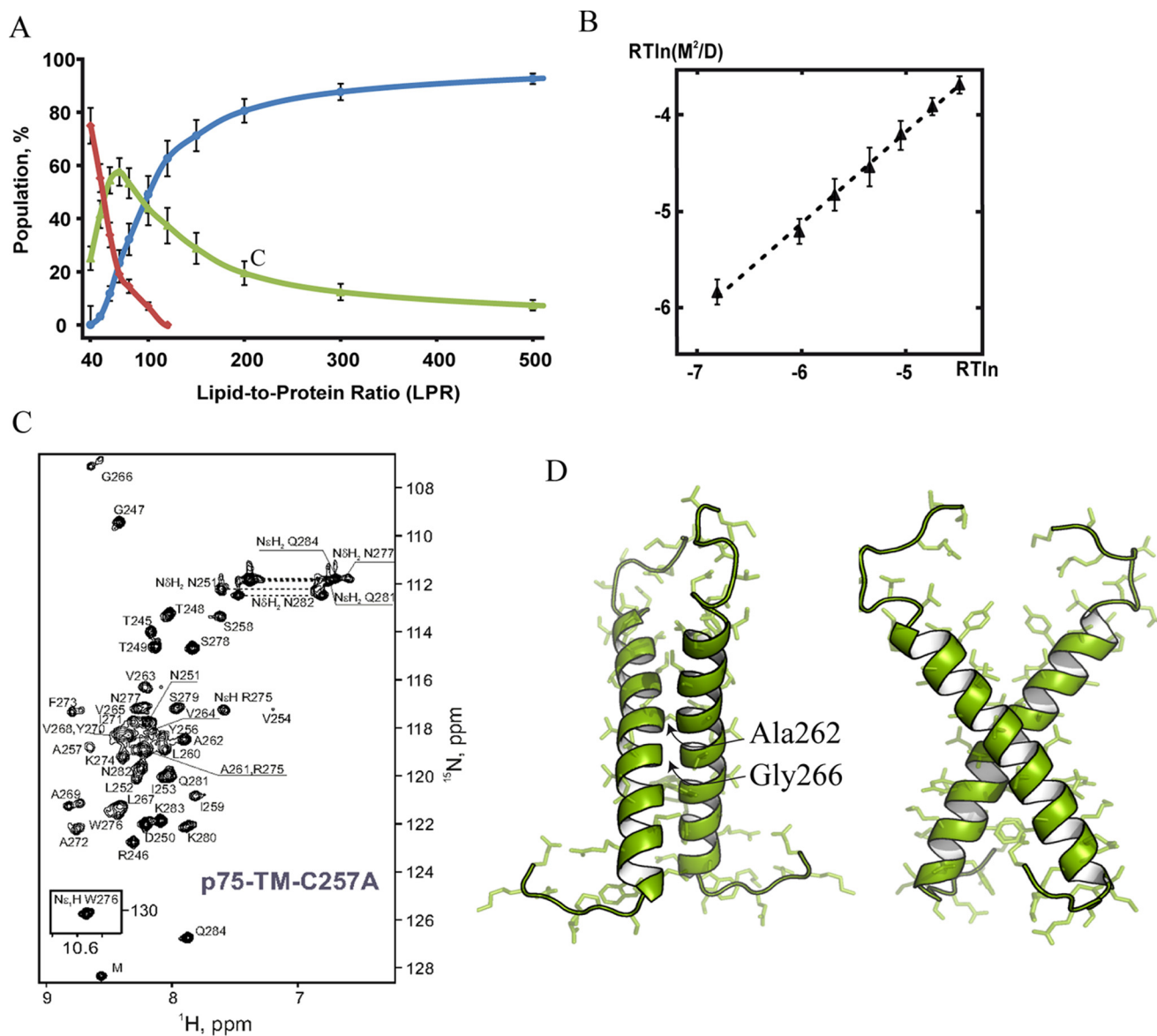
FIGURE 3. **Solution structure of the p75-TM-C257A dimer in DPC micelles.** *A*, percentage of the monomeric (*blue*), dimeric (*green*), and oligomeric (*red*) forms of p75-TM-C257A at different LPRs. Population values were calculated from the cross-peak intensities in the ^{1}H/^{15}N TROSY spectra. *B*, apparent free energy of dimerization of p75-TM-C257A. $\Delta G_{app} = RT\ln([M]2/[D])$ as a function $RT\ln(X)$ where $X = ([Det] - Nm[M] - Nd[D])/Ne$. $[M]$, $[D]$, and $[Det]$ represent monomer, dimer, and DPC concentration, respectively; Ne represents the number of DPC molecules per empty micelle; and Nm and Nd represent the number of DPC molecules per micelle containing monomer and dimer, respectively. *C*, ^{1}H/^{15}N HSQC spectrum of p75-TM-C257A solubilized in an aqueous suspension of DPC micelles at an LPR of 50:1, 45 °C, and pH 5.9. ^{1}H-^{15}N backbone and side-chain resonance assignments are shown. *D*, schematic representation of the spatial structure of the p75-TM-C257A dimer from two different angles; front, 90° rotation. TM helices are represented as *ribbons*, and side chains are represented as *sticks*. The Protein Data Bank accession code for p75-TM-C257A is 2mjo. *Error bars* represent S.E.

juxtamembrane region is present in the protein construct (56). In our case, the juxtamembrane regions are absent, so we can deem our data as reliable.

Although solution NMR is usually used to determine the structure of TM domains, recently solid-state NMR approaches proved to be efficient to determine the correct TM domain topology, tilt, and TM-TM domain contacts in even more native environment such as lipid bilayers (49–52). We think that solid-state NMR may be the method of choice to study the orientation of the TM helix, but studies of helix-helix interactions in dimers may be not feasible. To our knowledge, there is only one successful attempt to resolve the structure of a helical dimer in bilayers by solid-state NMR (55). This attempt

required a very expensive and time-consuming scheme of isotope labeling and was accomplished with glycophorin A, which is a remarkably stable dimer. In a case where both monomer and dimer states were abundant and when there were motions on the dimerization interface, such work would be impossible.

The structure of the p75 TM disulfide dimer that we describe here sheds light on several aspects of p75 activation. Our experiments showed that disulfide bonds are spontaneously formed upon dimer formation. However, according to the TM domain structure, Cys[257] is in the first turn of the α-helix, and therefore it will reside close to the lipid-water interface in a real bilayer, accessible to the aqueous environment necessary for the formation of the disulfide bond. Our studies on the isolated TM
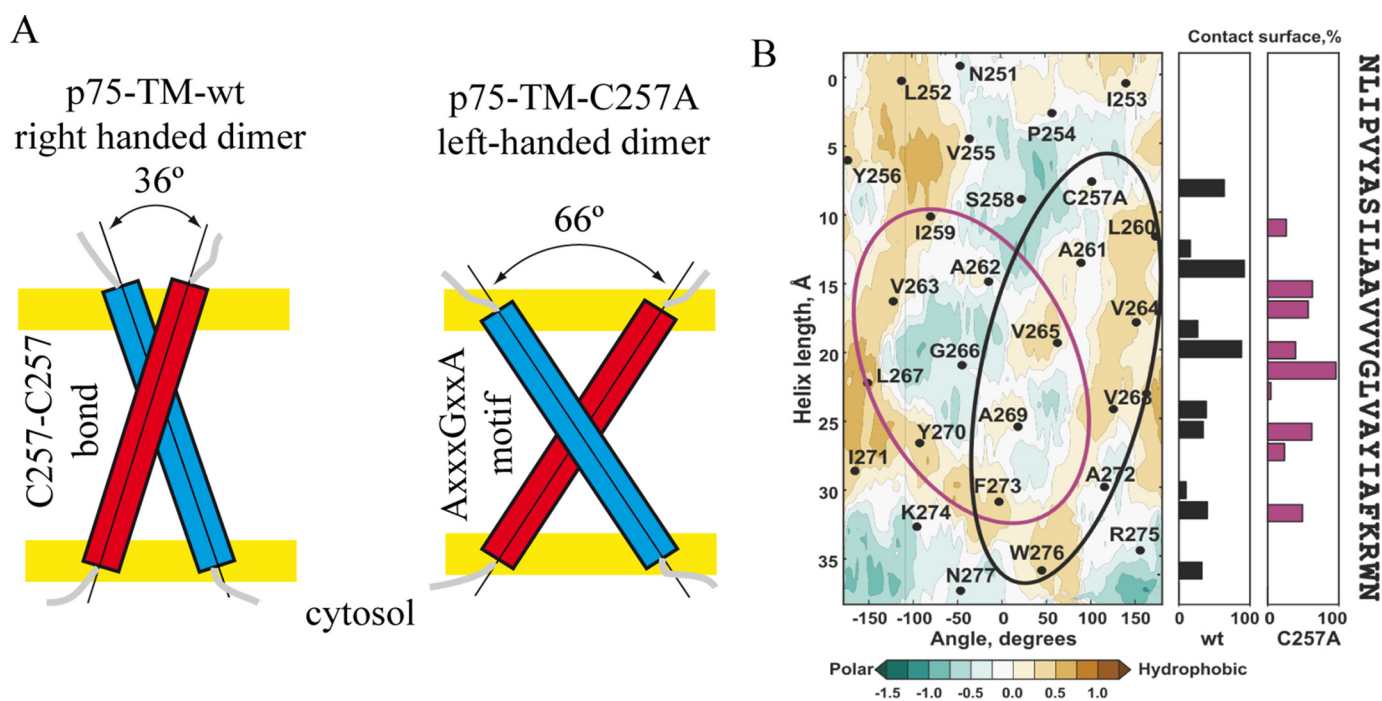
FIGURE 4. **Different dimer conformations in p75-TM-WT and p75-TM-C257A.** *A*, schematic illustration of the p75-TM-WT and p75-TM-C257A TM domains. *B*, hydrophobicity map for the p75-TM-WT and p75-TM-C257A helix surface, calculated using PREDDIMER. Helix-packing interfaces are indicated with *ovals*. *Black* and *magenta ovals* indicate the residues comprising the p75-TM-WT and p75-TM-C257A dimerization interfaces, respectively. The *two panels* to the *right* show the percentage of intermonomer contact surface area.

domain suggest that the dimerization of the transmembrane domain *per se* is triggering the disulfide bond formation; once two p75 TM domains dimerize, there is a high probability that the disulfide bond is formed. In support of this, we observed the presence of p75-TM-WT dimers in the absence of a disulfide bond in an oxygen-free atmosphere and in the presence of reducing agents, suggesting that the disulfide bond stabilizes an otherwise weak TM dimer. However, in the context of the full-length p75, this situation may be different, and the extracellular or intracellular domains may modulate the rotation of the TM domain in the plasma membrane to favor a specific interface.

Previously, an alternative *in silico* model of the p75 TM dimer based on the glycophorin A (GpA) structure was proposed (9). The model was built by threading the p75 TM sequence on the structure of GpA dimer based on the assumption that the A*XXX*G motif in p75-WT is mediating the dimerization as does the G*XXX*G in the GpA dimer (57). However, the G*XXX*G-like motifs do not always participate in the TM domain dimerization (46) as we showed here for p75-TM-WT. In addition, p75 TM domain shares less than 10% of the protein sequence with GpA, suggesting that drawing conclusions from such a model may be risky. Our experimental data suggest that the model is probably wrong because under our experimental conditions p75-TM-WT forms the disulfide-bonded dimers and not A*XXX*G dimers.

Our structural and functional analysis suggests that the mutation C257A induces an essential rearrangement of the p75 TM dimer. NMR titration experiments suggest that Cys[257] is located on the dimer interface in both the disulfide-linked and non-covalent dimers. Cysteine residues may participate in hydrogen bond formation both intra- and intermolecularly (58). In several protein structures, hydrogen bonds are found

between the sulfhydryl group of cysteine residue *i* and the carbonyl oxygen of residue *i − 4*, and they play an important role in stabilizing the α-helix (58). In addition, reduced cysteine-cysteine pairs form a dual hydrogen bond, contributing to a higher stability of the dimer interface (58). Mutation of the Cys[257] will preclude the formation of these hydrogen bonds and may distort the α-helix structure, favoring a different dimer interface. To our understanding, the different conformations of p75-WT and p75-C257A provide a structural explanation to the results showing that p75-C257A is inactive and its impact on receptor intramembrane proteolysis. However, it raises the concern that p75-C257A is actually not reflecting a native conformation of p75-WT, and care must be taken in extrapolating some of the activities of p75-C257A to interrogate p75 signaling.

We confirmed previous observations that mutation of the A*XXX*G motif contributes to a reduced cleavage catalyzed by the γ-secretase complex (9). Interestingly, G*XXX*G motifs are needed for the binding of the γ-secretase complex to the amyloid precursor protein (59). Although the recognition mechanism by which the γ-secretase binds to its substrates is still unknown, based on the fact that A[262]VV ↓ VG[266] motif of p75 is part of the target site for the γ-secretase cleavage (60), the most plausible explanation is that mutations in this region would induce a local conformational change in the α-helix with a negative impact on cleavage rather than mediating a protein-protein interaction. Recently mutation of the Val[264] impaired the cleavage by γ-secretase, supporting this hypothesis (49). In p75-C257A, the A*XXX*G motif is participating in the homodimer formation and is less accessible to the γ-secretase complex (Fig. 6*E*). This together with the different and probably

A

```
wt-    NLIPVYCSILAAVVVGLVAYIAFKRW
C257A-NLIPVYASILAAVVVGLVAYIAFKRW
C257S-NLIPVYSSILAAVVVGLVAYIAFKRW
C257I-NLIPVYISILAAVVVGLVAYIAFKRW
A261I-NLIPVYCSILIAVVVGLVAYIAFKRW
A262I-NLIPVYCSILAIVVVGLVAYIAFKRW
G266I-NLIPVYCSILAAVVVILVAYIAFKRW
AGA   -NLIPVYCSILAIVVVILVAYIIFKRW
C/G   -NLIPVYASILAAVVVILVAYIAFKRW
C/AGA-NLIPVYASILAIVVVILVAYIIFKRW
```
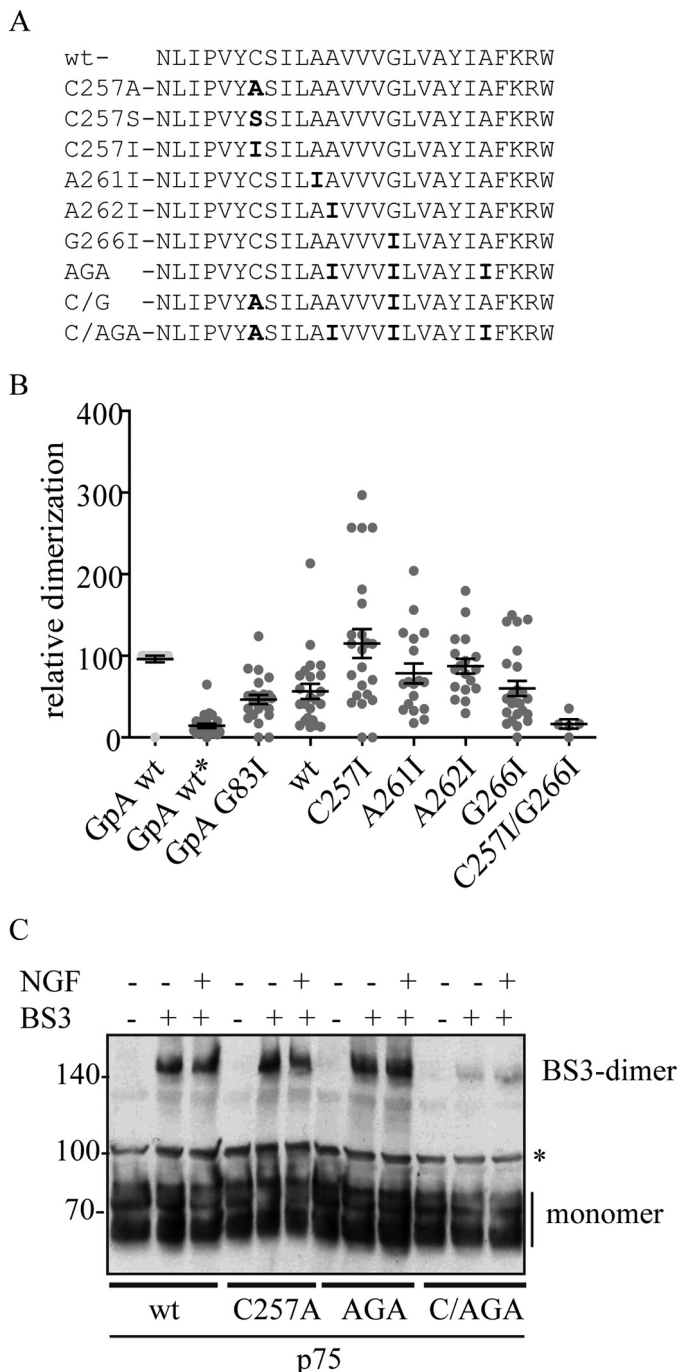
B

C

FIGURE 5. **Dimerization of p75 by ToxRED and in mammalian cells.** *A*, sequences of the p75 TM mutant constructs used. The mutated residue is shown in *bold*. *B, left*, percentage of dimerization, normalized to GpA-WT (100%), of p75-TM-WT and p75 TM mutants (results represent the average of at least 10 colonies analyzed in triplicate). GpA-wt* is a ToxRED negative control with a mutation in the ToxR protein (33). *C, in vivo* cross-linking of full-length p75 mutants in transfected HeLa cells. NGF (10 ng/ml) was used in the lanes indicated. Cells were lysed in the presence of iodoacetamide, subjected to reducing SDS-PAGE, and then immunoblotted and probed with a specific p75 antibody against p75-ICD. *Error bars* represent S.E. *BS3*, bis(sulfosuccinimidyl)suberate. * refers to non-specific protein band.

non-native conformation of the C257A dimer may contribute to the reduced cleavage observed in this mutant.

Based on the functional data showing that the disulfide dimers are required for the receptor activation, an important question to answer is when and how they are formed. It is plau-

sible that most of the p75 in the membrane is in the form of a homodimer or a heterodimer with another co-receptor. The conformation imposed by the disulfide bond may release an inhibitory state or lock a specific conformation necessary for better positioning of the intracellular domain of p75 to bind the effector proteins or the extracellular domain to bind the NTs more efficiently. Actually a preformed dimer will increase the affinity for its ligand quantitatively.

How a disulfide-linked dimer is able to transduce the signaling after NGF binding is still an unsolved issue. A conformational model, as some of us proposed previously (8), is difficult to imagine based on the restricted movement of a covalent dimer and the intrinsic disorder of the juxtamembrane domain of p75 (21). Alternatively, we propose that binding of NGF may induce lateral interactions between several p75 disulfide-linked dimers to form clusters. Clustering may be formed by extracellular domain and/or ICD interactions and will promote an increase in the affinity of the protein-protein interactions taking place in p75 signaling with proteins containing death domains, caspase recruitment domains, and TNF receptor-associated factor domains. It is expected that up-regulation of p75 and the subsequent increase in p75 concentration at the membrane will favor TM dimerization and the formation of more disulfide-linked dimers. This may explain why elevated levels of p75 are usually toxic by overexpression or after trauma (3, 61). However, in homeostatic conditions, p75 TM dimerization may be regulated by different mechanisms as different cell types do not contain equivalent amounts of p75 disulfide dimers despite showing similar p75 expression levels (8). Interaction of p75 with other proteins that mask or block the accessibility of the Cys[257] could be one mechanism. As an example of this, we recently described the formation of a covalent heterodimer between the Cys[257] of p75 and the homologous Cys[58] of p45/NRH2 that blocks the formation and signaling of the disulfide homodimer of p75 (17). Other co-receptors, like TrkA, sortilin, and Nogo receptor, that are reported to complex with p75 (62–64) are candidates to modulate p75 dimerization as well. This adds to the complexity of p75 TM dimer regulation.

Recently it has been proposed that p75 exists in the membrane as a monomer and a trimer (10). The authors proposed that p75 disulfide dimers are needed to bind another molecule of p75 via the extracellular domain. Although the authors rely exclusively on abnormally migrating bands on SDS-PAGE to discern the stoichiometry, we cannot exclude that p75 disulfide dimers may form oligomers with other copies of p75 *in vivo*. However, to be observed in SDS-PAGE, these interactions need to be SDS-resistant and take place outside of the TM domain as we never detected a trimer species in our hands. That possibility is difficult to understand in the absence of more biochemical data describing the nature of such strong protein-protein interactions and taking into account that the "gel shifting" of membrane proteins in SDS-PAGE is conformation-dependent (65). Alternatively p75 disulfide dimers may bind to other components of the plasma membrane and contribute to the abnormal migration in SDS-PAGE. For instance, SDS-resistant aggregates of p75 with components of the plasma membrane, like gangliosides, have been described previously (66).
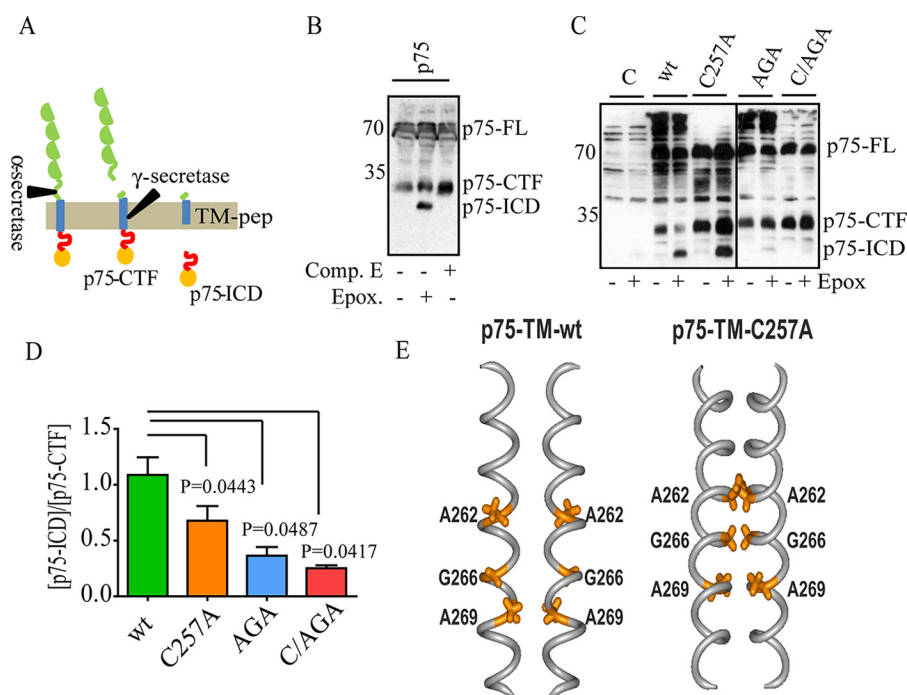
FIGURE 6. **p75 cleavage is influenced by transmembrane domain conformation: role of the A***XXX*G*XX*A motif. *A*, p75 undergoes regulated intramembrane proteolysis mediated sequentially by α- and γ-secretase activity. *B*, Western blot showing the cleavage of p75-WT and p75-C257A constructs in transfected HeLa cells in the presence of PMA. Protein bands corresponding to p75 full length (*FL*), p75-CTF, and p75-ICD are indicated. *C*, Western blot showing cleavage of p75-WT and p75 mutants in transfected HeLa cells in the presence of PMA. *D*, quantification of at least three different experiments as shown in *C*; the graph plots the p75-ICD:p75-CTF ratio. Significant differences were determined by one-way analysis of variance, comparing all mutants with p75-WT. *p* values are shown. Significance with 95% confidence interval is defined as $p < 0.05$. *E*, α-helix models of p75-TM-WT (*left*) and p75-TM-C257A (*right*) dimers, highlighting the position of the A^{262}*XXX*G^{266}*XX*A^{269} dimerization motif (*orange*). *Error bars* represent S.E. *C*, control; *dim*, dimer; *TM-pep*, TM peptide; *Comp. E*, Compound E; *Epox.*, epoxomicin.

To conclude, during the preparation of this manuscript, the structure of the trimer of Fas transmembrane domain was reported (67). Although p75 was the founding member of the TNF receptor superfamily (68, 69), in several respects p75 is an atypical member. Most TNF receptor proteins signal in trimeric form and are activated by trimeric TNF-like ligands, whereas p75 forms dimers and is activated by dimeric NTs that are structurally unrelated to the TNF-like ligands (69). Our structural studies presented here add another exclusive characteristic of p75 among the TNF receptor superfamily members and confirm a considerable amount of data supporting the dimeric nature of p75.

Author Contributions—S. A. G. developed the expression protocols and synthesized samples for NMR analysis. K. D. N. designed and performed NMR experiments and analyzed NMR data. K. S. M. analyzed NMR data and contributed to the preparation of the manuscript. I. G.-C. prepared all p75 mutants and performed the ToxRED and p75 cleavage experiments. A. S. A. and M. V. designed and supervised the entire project and wrote the manuscript.

References

1. Friedman, W. J., and Greene, L. A. (1999) Neurotrophin signaling via Trks and p75. *Exp. Cell Res.* **253,** 131–142
2. Liepinsh, E., Ilag, L. L., Otting, G., and Ibáñez, C. F. (1997) NMR structure of the death domain of the p75 neurotrophin receptor. *EMBO J.* **16,** 4999–5005
3. Ibáñez, C. F., and Simi, A. (2012) p75 neurotrophin receptor signaling in nervous system injury and degeneration: paradox and opportunity. *Trends Neurosci.* **35,** 431–440
4. Yamashita, T., Fujitani, M., Hata, K., Mimura, F., and Yamagishi, S. (2005) Diverse functions of the p75 neurotrophin receptor. *Anat. Sci. Int.* **80,** 37–41
5. Nykjaer, A., Willnow, T. E., and Petersen, C. M. (2005) p75NTR—live or let die. *Curr. Opin. Neurobiol.* **15,** 49–57
6. Roux, P. P., and Barker, P. A. (2002) Neurotrophin signaling through the p75 neurotrophin receptor. *Prog. Neurobiol.* **67,** 203–233
7. Vilar, M., Charalampopoulos, I., Kenchappa, R. S., Reversi, A., Klos-Applequist, J. M., Karaca, E., Simi, A., Spuch, C., Choi, S., Friedman, W. J., Ericson, J., Schiavo, G., Carter, B. D., and Ibáñez, C. F. (2009) Ligand-independent signaling by disulfide-crosslinked dimers of the p75 neurotrophin receptor. *J. Cell Sci.* **122,** 3351–3357
8. Vilar, M., Charalampopoulos, I., Kenchappa, R. S., Simi, A., Karaca, E., Reversi, A., Choi, S., Bothwell, M., Mingarro, I., Friedman, W. J., Schiavo, G., Bastiaens, P. I., Verveer, P. J., Carter, B. D., and Ibáñez, C. F. (2009) Activation of the p75 neurotrophin receptor through conformational rearrangement of disulphide-linked receptor dimers. *Neuron* **62,** 72–83
9. Sykes, A. M., Palstra, N., Abankwa, D., Hill, J. M., Skeldal, S., Matusica, D., Venkatraman, P., Hancock, J. F., and Coulson, E. J. (2012) The effects of transmembrane sequence and dimerization on cleavage of the p75 neurotrophin receptor by gamma-secretase. *J. Biol. Chem.* **287,** 43810–43824
10. Anastasia, A., Barker, P. A., Chao, M. V., and Hempstead, B. L. (2015) Detection of p75NTR trimers: implications for receptor stoichiometry and activation. *J. Neurosci.* **35,** 11911–11920
11. Wiesmann, C., and de Vos, A. M. (2001) Nerve growth factor: structure and function. *Cell. Mol. Life Sci.* **58,** 748–759
12. Grob, P. M., Berlot, C. H., and Bothwell, M. A. (1983) Affinity labeling and partial purification of nerve growth factor receptors from rat pheochro-

mocytoma and human melanoma cells. *Proc. Natl. Acad. Sci. U.S.A.* **80**, 6819–6823

13. Gong, Y., Cao, P., Yu, H. J., and Jiang, T. (2008) Crystal structure of the neurotrophin-3 and p75NTR symmetrical complex. *Nature* **454**, 789–793

14. Feng, D., Kim, T., Ozkan, E., Light, M., Torkin, R., Teng, K. K., Hempstead, B. L., and Garcia, K. C. (2010) Molecular and structural insight into proNGF engagement of p75NTR and sortilin. *J. Mol. Biol.* **396**, 967–984

15. Aurikko, J. P., Ruotolo, B. T., Grossmann, J. G., Moncrieffe, M. C., Stephens, E., Leppänen, V. M., Robinson, C. V., Saarma, M., Bradshaw, R. A., and Blundell, T. L. (2005) Characterization of symmetric complexes of nerve growth factor and the ectodomain of the pan-neurotrophin receptor, p75NTR. *J. Biol. Chem.* **280**, 33453–33460

16. He, X. L., and Garcia, K. C. (2004) Structure of nerve growth factor complexed with the shared neurotrophin receptor p75. *Science* **304**, 870–875

17. Vilar, M., Sung, T. C., Chen, Z., García-Carpio, I., Fernandez, E. M., Xu, J., Riek, R., and Lee, K. F. (2014) Heterodimerization of p45-p75 modulates p75 signaling: structural basis and mechanism of action. *PLos Biol.* **12**, e1001918

18. Lin, Z., Tann, J. Y., Goh, E. T., Kelly, C., Lim, K. B., Gao, J. F., and Ibanez, C. F. (2015) Structural basis of death domain signaling in the p75 neurotrophin receptor. *eLife* **4**, e11692

19. Wehrman, T., He, X., Raab, B., Dukipatti, A., Blau, H., and Garcia, K. C. (2007) Structural and mechanistic insights into nerve growth factor interactions with the TrkA and p75 receptors. *Neuron* **53**, 25–38

20. Jiang, G., and Hunter, T. (1999) Receptor signaling: when dimerization is not enough. *Curr. Biol.* **9**, R568–R571

21. Mineev, K. S., Goncharuk, S. A., Kuzmichev, P. K., Vilar, M., and Arseniev, A. S. (2015) NMR dynamics of transmembrane and intracellular domains of p75NTR in lipid-protein nanodiscs. *Biophys. J.* **109**, 772–782

22. Aoki, M., Matsuda, T., Tomo, Y., Miyata, Y., Inoue, M., Kigawa, T., and Yokoyama, S. (2009) Automated system for high-throughput protein production using the dialysis cell-free method. *Protein Expr. Purif.* **68**, 128–136

23. Kai, L., Roos, C., Haberstock, S., Proverbio, D., Ma, Y., Junge, F., Karbyshev, M., Dötsch, V., and Bernhard, F. (2012) Systems for the cell-free synthesis of proteins. *Methods Mol. Biol.* **800**, 201–225

24. Schwarz, D., Junge, F., Durst, F., Frölich, N., Schneider, B., Reckel, S., Sobhanifar, S., Dötsch, V., and Bernhard, F. (2007) Preparative scale expression of membrane proteins in *Escherichia coli*-based continuous exchange cell-free systems. *Nat. Protoc.* **2**, 2945–2957

25. Schägger, H., and von Jagow, G. (1987) Tricine-sodium dodecyl sulfate-polyacrylamide gel electrophoresis for the separation of proteins in the range from 1 to 100 kDa. *Anal. Biochem.* **166**, 368–379

26. Goncharuk, S. A., Goncharuk, M. V., Mayzel, M. L., Lesovoy, D. M., Chupin, V. V., Bocharov, E. V., Arseniev, A. S., and Kirpichnikov, M. P. (2011) Bacterial synthesis and purification of normal and mutant forms of human FGFR3 transmembrane segment. *Acta Naturae* **3**, 77–84

27. Keller, R. L. J. (2004) *The Computer Aided Resonance Assignment Tutorial*, CANTINA Verlag, Goldau, Switzerland

28. Cavanagh, J., Fairbrother, W. J., Palmer, A. G., and Skelton, N. J. (2006) *Protein NMR Spectroscopy: Principles and Practice*, 2nd Ed., Academic Press, San Diego, CA

29. Güntert, P. (2004) Automated NMR structure calculation with CYANA. *Methods Mol. Biol.* **278**, 353–378

30. Shen, Y., and Bax, A. (2013) Protein backbone and sidechain torsion angles predicted from NMR chemical shifts using artificial neural networks. *J. Biomol. NMR* **56**, 227–241

31. Koradi, R., Billeter, M., and Wuthrich, K. (1996) MOLMOL: a program for display and analysis of macromolecular structures. *J. Mol. Graph.* **14**, 51–55, 29–32

32. Polyansky, A. A., Chugunov, A. O., Volynsky, P. E., Krylov, N. A., Nolde, D. E., and Efremov, R. G. (2014) PREDDIMER: a web server for prediction of transmembrane helical dimers. *Bioinformatics* **30**, 889–890

33. Berger, B. W., Kulp, D. W., Span, L. M., DeGrado, J. L., Billings, P. C., Senes, A., Bennett, J. S., and DeGrado, W. F. (2010) Consensus motif for integrin transmembrane helix association. *Proc. Natl. Acad. Sci. U.S.A.* **107**, 703–708

34. Kanning, K. C., Hudson, M., Amieux, P. S., Wiley, J. C., Bothwell, M., and Schecterson, L. C. (2003) Proteolytic processing of the p75 neurotrophin receptor and two homologs generates C-terminal fragments with signaling capability. *J. Neurosci.* **23**, 5425–5436

35. Mineev, K. S., Lesovoy, D. M., Usmanova, D. R., Goncharuk, S. A., Shulepko, M. A., Lyukmanova, E. N., Kirpichnikov, M. P., Bocharov, E. V., and Arseniev, A. S. (2014) NMR-based approach to measure the free energy of transmembrane helix-helix interactions. *Biochim. Biophys. Acta* **1838**, 164–172

36. Chen, L., Novicky, L., Merzlyakov, M., Hristov, T., and Hristova, K. (2010) Measuring the energetics of membrane protein dimerization in mammalian membranes. *J. Am. Chem. Soc.* **132**, 3628–3635

37. Fisher, L. E., Engelman, D. M., and Sturgis, J. N. (2003) Effect of detergents on the association of the glycophorin a transmembrane helix. *Biophys. J.* **85**, 3097–3105

38. Fleming, K. G. (2002) Standardizing the free energy change of transmembrane helix-helix interactions. *J. Mol. Biol.* **323**, 563–571

39. Bocharov, E. V., Mineev, K. S., Goncharuk, M. V., and Arseniev, A. S. (2012) Structural and thermodynamic insight into the process of "weak" dimerization of the ErbB4 transmembrane domain by solution NMR. *Biochim. Biophys. Acta* **1818**, 2158–2170

40. Bocharov, E. V., Lesovoy, D. M., Goncharuk, S. A., Goncharuk, M. V., Hristova, K., and Arseniev, A. S. (2013) Structure of FGFR3 transmembrane domain dimer: implications for signaling and human pathologies. *Structure* **21**, 2087–2093

41. Russ, W. P., and Engelman, D. M. (2000) The GxxxG motif: a framework for transmembrane helix-helix association. *J. Mol. Biol.* **296**, 911–919

42. Fink, A., Sal-Man, N., Gerber, D., and Shai, Y. (2012) Transmembrane domains interactions within the membrane milieu: principles, advances and challenges. *Biochim. Biophys. Acta* **1818**, 974–983

43. Walters, R. F., and DeGrado, W. F. (2006) Helix-packing motifs in membrane proteins. *Proc. Natl. Acad. Sci. U.S.A.* **103**, 13658–13663

44. Polyansky, A. A., Volynsky, P. E., and Efremov, R. G. (2012) Multistate organization of transmembrane helical protein dimers governed by the host membrane. *J. Am. Chem. Soc.* **134**, 14390–14400

45. Russ, W. P., and Engelman, D. M. (1999) TOXCAT: a measure of transmembrane helix association in a biological membrane. *Proc. Natl. Acad. Sci. U.S.A.* **96**, 863–868

46. Teese, M. G., and Langosch, D. (2015) Role of GxxxG motifs in transmembrane domain interactions. *Biochemistry* **54**, 5125–5135

47. Kenchappa, R. S., Tep, C., Korade, Z., Urra, S., Bronfman, F. C., Yoon, S. O., and Carter, B. D. (2010) p75 neurotrophin receptor-mediated apoptosis in sympathetic neurons involves a biphasic activation of JNK and up-regulation of tumor necrosis factor-α-converting enzyme/ADAM17. *J. Biol. Chem.* **285**, 20358–20368

48. Kenchappa, R. S., Zampieri, N., Chao, M. V., Barker, P. A., Teng, H. K., Hempstead, B. L., and Carter, B. D. (2006) Ligand-dependent cleavage of the p75 neurotrophin receptor is necessary for NRIF nuclear translocation and apoptosis in sympathetic neurons. *Neuron* **50**, 219–232

49. Vicario, A., Kisiswa, L., Tann, J. Y., Kelly, C. E., and Ibáñez, C. F. (2015) Neuron-type-specific signaling by the p75NTR death receptor regulated by differential proteolytic cleavage. *J. Cell Sci.* **128**, 1507–1517

50. Skeldal, S., Matusica, D., Nykjaer, A., and Coulson, E. J. (2011) Proteolytic processing of the p75 neurotrophin receptor: a prerequisite for signalling?: neuronal life, growth and death signalling are crucially regulated by intramembrane proteolysis and trafficking of p75(NTR). *BioEssays* **33**, 614–625

51. Nakano, M., Fukuda, M., Kudo, T., Miyazaki, M., Wada, Y., Matsuzaki, N., Endo, H., and Handa, T. (2009) Static and dynamic properties of phospholipid bilayer nanodiscs. *J. Am. Chem. Soc.* **131**, 8308–8312

52. Mineev, K. S., Bocharov, E. V., Volynsky, P. E., Goncharuk, M. V., Tkach, E. N., Ermolyuk, Y. S., Schulga, A. A., Chupin, V. V., Maslennikov, I. V., Efremov, R. G., and Arseniev, A. S. (2011) Dimeric structure of the transmembrane domain of glycophorin a in lipidic and detergent environments. *Acta Naturae* **3**, 90–98

53. Bocharov, E. V., Pustovalova, Y. E., Pavlov, K. V., Volynsky, P. E., Goncharuk, M. V., Ermolyuk, Y. S., Karpunin, D. V., Schulga, A. A., Kirpichnikov, M. P., Efremov, R. G., Maslennikov, I. V., and Arseniev, A. S. (2007)

Unique dimeric structure of BNip3 transmembrane domain suggests membrane permeabilization as a cell death trigger. *J. Biol. Chem.* **282,** 16256–16266

54. Sulistijo, E. S., and Mackenzie, K. R. (2009) Structural basis for dimerization of the BNIP3 transmembrane domain. *Biochemistry* **48,** 5106–5120

55. Smith, S. O., Song, D., Shekar, S., Groesbeek, M., Ziliox, M., and Aimoto, S. (2001) Structure of the transmembrane dimer interface of glycophorin A in membrane bilayers. *Biochemistry* **40,** 6553–6558

56. Mineev, K. S., Panova, S. V., Bocharova, O. V., Bocharov, E. V., and Arseniev, A. S. (2015) The membrane mimetic affects the spatial structure and mobility of EGFR transmembrane and juxtamembrane domains. *Biochemistry* **54,** 6295–6298

57. MacKenzie, K. R., Prestegard, J. H., and Engelman, D. M. (1997) A transmembrane helix dimer: structure and implications. *Science* **276,** 131–133

58. Zhou, P., Tian, F., Lv, F., and Shang, Z. (2009) Geometric characteristics of hydrogen bonds involving sulfur atoms in proteins. *Proteins* **76,** 151–163

59. Mao, G., Tan, J., Cui, M. Z., Chui, D., and Xu, X. (2009) The GxxxG motif in the transmembrane domain of AβPP plays an essential role in the interaction of CTFβ with the γ-secretase complex and the formation of amyloid-β. *J. Alzheimers Dis.* **18,** 167–176

60. Jung, K. M., Tan, S., Landman, N., Petrova, K., Murray, S., Lewis, R., Kim, P. K., Kim, D. S., Ryu, S. H., Chao, M. V., and Kim, T. W. (2003) Regulated intramembrane proteolysis of the p75 neurotrophin receptor modulates its association with the TrkA receptor. *J. Biol. Chem.* **278,** 42161–42169

61. Bhakar, A. L., Howell, J. L., Paul, C. E., Salehi, A. H., Becker, E. B., Said, F., Bonni, A., and Barker, P. A. (2003) Apoptosis induced by p75NTR overexpression requires Jun kinase-dependent phosphorylation of Bad. *J. Neurosci.* **23,** 11373–11381

62. Wang, K. C., Kim, J. A., Sivasankaran, R., Segal, R., and He, Z. (2002) p75 interacts with the Nogo receptor as a co-receptor for Nogo, MAG and OMgp. *Nature* **420,** 74–78

63. Nykjaer, A., Lee, R., Teng, K. K., Jansen, P., Madsen, P., Nielsen, M. S., Jacobsen, C., Kliemannel, M., Schwarz, E., Willnow, T. E., Hempstead, B. L., and Petersen, C. M. (2004) Sortilin is essential for proNGF-induced neuronal cell death. *Nature* **427,** 843–848

64. Hempstead, B. L., Martin-Zanca, D., Kaplan, D. R., Parada, L. F., and Chao, M. V. (1991) High-affinity NGF binding requires coexpression of the trk proto-oncogene and the low-affinity NGF receptor. *Nature* **350,** 678–683

65. Rath, A., Glibowicka, M., Nadeau, V. G., Chen, G., and Deber, C. M. (2009) Detergent binding explains anomalous SDS-PAGE migration of membrane proteins. *Proc. Natl. Acad. Sci. U.S.A.* **106,** 1760–1765

66. Yamashita, T., Higuchi, H., and Tohyama, M. (2002) The p75 receptor transduces the signal from myelin-associated glycoprotein to Rho. *J. Cell Biol.* **157,** 565–570

67. Fu, Q., Fu, T. M., Cruz, A. C., Sengupta, P., Thomas, S. K., Wang, S., Siegel, R. M., Wu, H., and Chou, J. J. (2016) Structural basis and functional role of intramembrane trimerization of the Fas/CD95 death receptor. *Mol. Cell* **61,** 602–613

68. Johnson, D., Lanahan, A., Buck, C. R., Sehgal, A., Morgan, C., Mercer, E., Bothwell, M., and Chao, M. (1986) Expression and structure of the human NGF receptor. *Cell* **47,** 545–554

69. Bothwell, M. (2006) Evolution of the neurotrophin signaling system in invertebrates. *Brain Behav. Evol.* **68,** 124–132

≋ASBMB